



HAL
open science

Drought offsets the positive effect of summer heat waves on the canopy greenness of mountain grasslands

M.C. Corona-Lozada, Samuel Morin, Philippe Choler

► To cite this version:

M.C. Corona-Lozada, Samuel Morin, Philippe Choler. Drought offsets the positive effect of summer heat waves on the canopy greenness of mountain grasslands. *Agricultural and Forest Meteorology*, 2019, 276-277, pp.107617. 10.1016/j.agrformet.2019.107617. hal-02404398

HAL Id: hal-02404398

<https://hal.science/hal-02404398>

Submitted on 25 Oct 2021

HAL is a multi-disciplinary open access archive for the deposit and dissemination of scientific research documents, whether they are published or not. The documents may come from teaching and research institutions in France or abroad, or from public or private research centers.

L'archive ouverte pluridisciplinaire **HAL**, est destinée au dépôt et à la diffusion de documents scientifiques de niveau recherche, publiés ou non, émanant des établissements d'enseignement et de recherche français ou étrangers, des laboratoires publics ou privés.



Distributed under a Creative Commons Attribution - NonCommercial 4.0 International License

1 **Drought offsets the positive effect of summer heat waves on the canopy greenness of mountain**
2 **grasslands**

3

4

5 **M.C. Corona-Lozada¹, S. Morin² & P. Choler^{1,3}**

6 ¹ Univ. Grenoble Alpes, Univ. Savoie Mont Blanc, CNRS, LECA, F-38000 Grenoble, France

7 ² Univ. Grenoble Alpes, Université de Toulouse, Météo-France, CNRS, CNRM, Centre d'Études de
8 la Neige, F-38000 Grenoble, France

9 ³ Univ. Grenoble Alpes, Univ. Savoie Mont Blanc, CNRS, LTSER Zone Atelier Alpes, F-38000
10 Grenoble, France

11

12 Corresponding author: Philippe CHOLER

13 philippe.choler@univ-grenoble-alpes.fr

14 Tel: +33 4 76 51 48 96

15 ORCID : 0000-0002-9062-2721

16

17 **Keywords**

18 Climatic water balance; European Alps; heat wave; MODIS; mountain grasslands; phenology.

19 **Abstract (195 words)**

20 Heat waves are becoming more frequent in a warming climate and understanding the impacts
21 of these extreme events on terrestrial ecosystems remains a major challenge. Seasonally snow-
22 covered mountain grasslands are temperature-limited ecosystems and one may question whether the
23 summer heat waves there have the same negative effect on primary productivity as they have on
24 lowland ecosystems. Here, we examined the remotely-sensed phenology of mountain grasslands in
25 the French Alps with a particular focus on the four unusually warm summers that occurred in 2003,
26 2012, 2015, and 2016. Our results showed that an early and rapid senescence and a lack of late-
27 season regrowth were the most significant responses in 2003 and 2012 when heat waves coincided
28 with climatic water deficit, i.e. negative anomalies of precipitation minus reference
29 evapotranspiration. Mountain grasslands located below 2350m were the most affected. In contrast,
30 we found low senescence and moderate to high regrowth in 2015 and 2016 which were years
31 unaffected by severe water deficit. When water was non-limiting, warm and even very warm
32 summers have a positive effect on the canopy greenness of the highest grasslands, particularly by
33 extending the green period in late summer and early fall. Our study highlights the pivotal role that
34 summer water balance has in the phenological response of mountain grasslands exposed to heat
35 waves.

36

37 **Introduction**

38 There has been a marked increase in air temperature in the European Alps from the 1980s
39 onwards and this has caused warmer and longer snow-free periods for mountain vegetation (Durand
40 et al., 2009a; Gobiet et al., 2014; Beniston et al., 2018). A growing body of evidence indicates that
41 above treeline ecosystems have undergone significant changes over the last decades, including
42 changes in community composition (Gottfried et al., 2012; Cannone and Pignatti, 2014) and
43 ecosystem functioning (Choler, 2015). Many of these documented changes, such as the upward shift
44 of species (Lenoir et al., 2008; Steinbauer et al., 2018), the thermophilization of high summit flora
45 (Gottfried et al., 2012), or the long-term greening of vegetation at high elevation (Carlson et al.,
46 2017), are consistent with the expected positive effects of rising temperatures in temperature-limited
47 ecosystems. Nonetheless, recent reports indicate that earlier frost exposure due to the earlier snow
48 melt-out date (Wheeler et al., 2014; Liu et al., 2018), more frequent heat waves (Cremonese et al.,
49 2017) and droughts (Marchin et al., 2018) may be additional effects of on-going climate change
50 which could attenuate this positive response. These studies highlighted the need to consider both
51 trends and extreme events when assessing mountain vegetation response to climate change.

52 In a warming climate, the duration, intensity, and frequency of heat waves is expected to
53 markedly increase (Stocker et al., 2013). The few reports that examine the response of mountain
54 grasslands to summer heat waves have yielded contrasting results. Using both remote sensing and *in*
55 *situ* measurements, Jolly et al. (2005) found a positive effect of the 2003 heat wave on the summer
56 greenness of high-elevation ecosystems in the Swiss Alps, and this was in stark contrast with what
57 was happening in lowland ecosystems. Cremonese et al. (2017) used flux data and time-lapse
58 cameras to characterize the effect of the 2015 heat wave on a subalpine *Nardus*-rich community and
59 noted a reduction of canopy development in addition to advanced senescence. Experimental
60 approaches using monolith transplantation have highlighted that the negative effect of an increased
61 air temperature only occurred when it coincided with reduced water supply (De Boeck et al., 2016).

62 This calls for a comparative study that includes a broader range of temperature-precipitation
63 combinations to better capture the interplay of heat waves and drought on mountain grassland
64 phenology.

65 The remote sensing of vegetation phenology provides a unique opportunity to track ecosystem
66 responses to climate change at a regional scale and over decades (Pettorelli et al., 2005; Richardson
67 et al., 2013). In mountainous environments, several studies have successfully used high or medium
68 resolution satellite images to examine the relationships between climate and the growth response of
69 mountain grasslands (Fontana et al., 2008; Dunn and de Beurs, 2011; Zhang et al., 2013b; Choler,
70 2015). For seasonally snow-covered ecosystems, the use of snow and vegetation indices may provide
71 several phenological metrics including the onset of growth, the date and magnitude of maximum
72 canopy greenness, the dynamics of senescence, and the date of the first snowfalls. However, many
73 comparative studies (either inter-annual or inter-spatial comparisons) have focused on the maximum
74 or averaged summer greenness and, by doing so, have largely overlooked the late and end of season
75 phenology (Gallinat et al., 2015; Garonna et al., 2018). Yet extreme events occurring after the date of
76 peak standing biomass, such as heat wave or drought, may accelerate the senescence or diminish the
77 possibility of regrowth and this has important consequences for the management of mountain
78 pastures (Nettier et al., 2017). We believe that remotely-sensed phenological metrics that capture the
79 kinetics of both growth and senescence phases will provide a more comprehensive assessment of
80 mountain grassland responses to heat waves.

81 In this paper, we used time series of the Normalized Difference Vegetation Index (NDVI) for
82 the period 2000 - 2016 to examine how the phenology of mountain grasslands has been impacted by
83 the summer heat waves in 2003, 2012, 2015 and 2016. We performed our comparative analysis by
84 using the NDVI from Moderate-Resolution Imaging Spectroradiometer (MODIS) and
85 meteorological variables derived from the SAFRAN (Système d'Analyse Fournissant des
86 Renseignements Atmosphériques à la Neige) reanalysis system (Durand et al., 2009a, 2009b). We

87 focused on the French Alps for which the availability of high-resolution land cover data allowed us
88 to select MODIS pixels with predominant coverage of mountain grasslands. More specifically, we
89 addressed the following three sets of questions: (1) what was the intensity, duration, and timing of
90 summer heat waves in the French Alps from 2000 to 2016 and to what extent did these events
91 coincide with climatic water deficit, (2) what are the remotely-sensed indicators that best capture the
92 impact of extreme meteorological events on the phenology of mountain grasslands, and (3) how do
93 heat wave and water balance interfere on the growth and senescence of mountain grasslands?
94

95 **Materials and Methods**

96 The distribution of mountain grasslands in the French Alps was derived from a 10 m resolution
97 land cover map of France produced by the Centre d'Expertise Scientifique Occupation des sols,
98 downloadable at <http://osr-cesbio.ups-tlse.fr/~oso/> (Inglada et al., 2017). To obtain a binary map of
99 mountain grasslands, we aggregated the three land cover classes corresponding to meadows
100 (“pelouses”, code 34), heathlands (“landes ligneuses”, code 36) and grasslands (“prairies”, code
101 211). We noticed that the class “landes ligneuses” included a limited number of pixels and was not
102 very reliable due to the difficulty in distinguishing mountain low shrubs from nearby grasslands and
103 meadows. We calculated the percent cover of the aggregated class at a 250 m resolution to align with
104 the MODIS data, selecting those pixels with >90% cover and a mean elevation ranging from 1350 m
105 to 2550 m m a.s.l.. This yielded a total of 44,295 pixels which fall into four elevation bands (1350 m
106 - 1650 m, 1650 m - 1950 m, 1950 m - 2250 m, and 2250 m - 2550 m) and 23 SAFRAN massifs (Fig.
107 1 and Table S1). Pixel-based estimates were averaged by elevation band and massif. This resulted in
108 a table containing 87 combinations of elevation band and massif and 17 years (2000 - 2016). Annual
109 standardized anomalies were calculated from this table.

110 For meteorological data, we used the SAFRAN reanalysis that simulates surface conditions as
111 a function of elevation in 300 m increments and for 23 massifs of French Alps. These massifs were

112 defined for their climatological homogeneity in a previous spatial analysis of all weather data
 113 available for the French Alps (Durand et al., 2009a; 2009b). The SAFRAN reanalysis was evaluated
 114 against in-situ observations by Durand et al. (2009a) and is used for many real-time and
 115 climatological applications in the French mountain areas (e.g. Verfaillie et al., 2018). The period
 116 from 1981 to 2010 was set as a reference period to estimate standardized anomalies. For each
 117 MODIS pixel, we extracted all the required meteorological data to compute a Heat Wave Magnitude
 118 index, hereafter HWI, and a Reference Crop Evapotranspiration, hereafter ET_0 as described below..

119 We simplified the methodology proposed by Russo et al. (2014) to calculate a HWI that
 120 accounts for both magnitude and duration of heat waves. First, we identified days exhibiting a
 121 maximum temperature above a threshold value. For each day of year (DOY) i , we assembled a
 122 dataset (DS_i) comprising the daily Tmax values of the n days before and after day i for the 30 year-
 123 long reference period (1981-2010) according to Eq. 1

$$DS_i = \bigcup_{y=1981}^{2010} \bigcup_{i-n}^{i+n} Tmax_{y,i} \quad (1) \quad \begin{matrix} 124 \\ 125 \end{matrix}$$

126 where the symbol U denotes the union of values. The 80th percentile of DS_i defined the
 127 threshold value for day i . As in Russo et al. (2014), we chose $n = 15$ days to estimate the threshold.
 128 We examined the sensitivity of HWI to varying values of n . The relative change in HWI was
 129 predominantly less than 5% when comparing $n=15$ with $n=13$, and less than 10% when comparing
 130 $n=15$ with $n=11$ (Fig. S1). In all cases, the ranking of years was the same and the main findings of
 131 the study did not change. Second, we selected all episodes of at least three consecutive days during
 132 for which the maximum air temperature exceeded the threshold and summed the daily maximum
 133 temperature of each episode to obtain an unscaled magnitude of the heat wave. Finally, we summed
 134 the unscaled magnitudes of all heat waves occurring during the three periods of interest (see below)..
 135 Compared to Russo et al. (2014), we did not consider sub-heat waves and did not rescale heat wave
 136 magnitude into probability values.

137 ET_0 is a Penman–Monteith estimate of potential evapotranspiration of a reference crop surface
 138 that quantifies the evaporating demand of the atmosphere when water is not limiting. We followed
 139 the recommendations of the Food and Agricultural Organization (Allen et al., 1998) to compute ET_0
 140 (in mm day^{-1}) from weather data (Eq. 2).

$$ET_0 = \frac{0.408 \Delta (R_n - G) + \gamma \frac{900}{(T_m + 273)} u_2 (e_s - e_a)}{\Delta + \gamma(1 + 0.34u_2)} \quad (2)$$

141
 142 where R_n is the net radiation at crop surface ($\text{MJ m}^{-2} \text{day}^{-1}$), G is the soil heat flux density (MJ
 143 $\text{m}^{-2} \text{day}^{-1}$), T_m is mean daily air temperature at 2 m ($^{\circ}\text{C}$), u_2 is the wind speed at 2 m (m s^{-1}), e_s is
 144 saturation vapour pressure (kPa), e_a is the actual vapour pressure (kPa), Δ is the slope of vapour
 145 pressure curve ($\text{kPa } ^{\circ}\text{C}^{-1}$), and γ is the psychrometric constant ($\text{kPa } ^{\circ}\text{C}^{-1}$). The use of SAFRAN
 146 reanalysis to compute ET_0 according to Eq. 2 is described in Vannier and Braud (2012). The climatic
 147 water balance corresponding to the difference between precipitation (P) and reference crop
 148 evapotranspiration, hereafter $P-ET_0$, was taken as a proxy to assess the dry–wet conditions of a given
 149 period.

150 For each year, HWI and $P - ET_0$ were computed over three periods of interest: (i) the
 151 climatological summer (June, July and August), hereafter JJA, (ii) the growth phase defined as the 30
 152 days preceding the date of maximum observed NDVI, hereafter B30, and (iii) the senescent phase
 153 defined as the 60 days following the date of maximum observed NDVI, hereafter A60 (Fig. 2). We
 154 examined the sensitivity of the results to the length of the latter two periods and did not find any
 155 significant effect if periods were increased or decreased by 10 to 15 days.

156 Our remote sensing analysis was based on the surface reflectance acquired by MODIS, a
 157 sensor onboard Terra satellite. We downloaded the collection 6 of the MOD09Q1 products,
 158 corresponding to tile h18.v4 ($40\text{--}50^{\circ} \text{N}$, $0\text{--}15.6^{\circ} \text{E}$), from the Land Processes Distributed Active
 159 Archive Center (<https://e4ftl01.cr.usgs.gov/>). The 8-day composite at 250 m resolution, covering the
 160 period from 18 February 2000 to 27 December 2016, was processed following Choler (2015). To

161 summarize, re-projected surface reflectance values (ρ) in the red and near-infrared (NIR) bandwidths
162 were used to calculate a NDVI according to Eq. 3, keeping only reflectance values of optimum
163 quality (according to the MOD09Q1 Quality Control flag). Following Choler & al. (2010), we first
164 removed outliers defined as NDVI values that were two times larger or smaller than the average
165 value of the two preceding and the two following observations. Such sudden changes in NDVI are
166 inconsistent with the growth or senescence dynamics of mountain grasslands and may be due to
167 quality control issues, ephemeral snowfall during summer etc. Only 0.2% of the total NDVI values
168 were discarded at this step. Missing values and removed outliers were gap-filled using a cubic spline
169 interpolation. We then applied a Savitzky and Golay low pass filter in which the original data value
170 at time t_i was replaced by the value of a cubic polynomial fitted for $2n+1$ points, with n being the
171 number of time steps preceding or following t_i (Savitzky and Golay, 1964). Consistent with our
172 previous studies (Choler et al., 2010; 2015), we empirically found that a window size of seven days
173 (i.e. $n=3$) was able to track ecologically significant changes in NDVI while still able to reduce noise
174 in the NDVI time series efficiently. Finally, we used cubic splines to daily interpolate the NDVI time
175 series and to derive the following phenological metrics (Fig. 2): (i) the growth onset, hereafter Onset,
176 defined as the Julian day on which NDVI reached half its maximum, (ii) the NDVI maximum,
177 hereafter NDVImax, as a proxy for the maximum canopy greenness, (iii) the Julian day of
178 NDVImax, hereafter TNDVImax, as the date of the peak vegetation (iv) the absolute NDVI decrease
179 during the 60 days following NDVImax, hereafter SEN (A60), see Eq. 4 as a proxy for the canopy
180 senescence, and (v) the absolute NDVI increase during the 60 days following NDVImax, hereafter
181 REG (A60), see Eq. 5 as a proxy for the end-of-season regrowth..

$$NDVI = \frac{\rho_{NIR} - \rho_{Red}}{\rho_{NIR} + \rho_{Red}} \quad (3)$$

$$SEN_{A60} = \sum_{i=TNDVImax}^{TNDVImax+59} \text{abs}(\min(0, NDVI_{i+1} - NDVI_i)) \quad (4)$$

$$REG_A60 = \sum_{i=TNDVImax}^{TNDVImax+59} \max(0, NDVI_{i+1} - NDVI_i) \quad (5)$$

182

183 Pixel-based estimates of phenology were averaged by elevation band and massif in order to
 184 align with meteorological variables. For REG (A60) we transformed the raw values into binary data
 185 (zero or positive values) and we calculated the percent of pixels exhibiting regrowth for each
 186 combination of elevation band and massif.

187 Standard Major Axis (SMA) regression analysis was used to analyse the bivariate relationships
 188 between anomalies of phenology and to test the statistical significance of any deviation of the slope
 189 from unity and of the intercept from zero (Warton and Ormerod, 2007). We modelled anomalies of
 190 NDVImax, SEN (A60) and REG (A60) as a linear function of anomalies of HWI and P-ET₀. The
 191 model was written as follows (Eq. 6)

$$anom(Y_z) = \beta_{0,z} + \beta_{1,z} anom(P - ET_0)_z + \beta_{2,z} anom(HWI)_z + \varepsilon_z \quad (6)$$

192

193 where Y is the dependent variable (phenology), β are the regression coefficients, $anom$ means
 194 standardized anomaly and ε is an error term. The β parameters were solved separately for each
 195 elevation band (z) using ordinary least squares regression.

196 All statistical analyses were performed in R (R Core Team, 2017), using the *signal* library
 197 (signal developers, 2013) for the time series analyses and the *raster* library (Hijmans, 2017) for the
 198 spatial analysis. All figures were produced using the *ggplot2* (Wickham, 2016) and the *rasterVis*
 199 (Perpinan Lamigueiro and Hijmans, 2018) libraries.

200

201 **Results**

202 Since the 1980s, warm to very warm summers with above normal HWI have become more
203 frequent in the French Alps (Fig. 3A). The four summers with the highest HWI all occurred in the
204 last 15 years, i.e. during the years 2003, 2012, 2015 and 2016 (Fig. 3A). The intensity of summer
205 heat waves reached a maximum in 2003 with an HWI (JJA) median value of 184 for the 1950 m -
206 2250 m elevation band (Fig. S2A). During the same period, we found a wide range of water balance
207 conditions during the summer period, with years when high values of HWI and negative P-ET₀
208 values co-occurred and other years when they occurred independently (Fig. 3, Fig. S2B). Summer
209 droughts coincided with the 2003 and 2012 heat waves, while summer water balance was close to
210 normal in 2015 and 2016 (Fig. 3B). The French Alps also experienced a severe drought in 2009, but
211 this was not accompanied by a significant heat wave (Fig. 3B).

212 Figure 4 showed that the 2012 and 2016 heat waves mainly concerned the late season while
213 those of 2003 and 2015 occurred throughout the growing season. Noticeably, there was no negative
214 anomaly of P-ET₀ before the peak of biomass in 2015 (Fig. 4A) and only a moderate one after the
215 peak (Fig. 4B). By comparison, the 2003, 2012 and 2016 late season heat waves co-occurred with
216 dry conditions, with the most adverse situations taking place in 2003 and 2012 (Fig. 4B).

217 Plant growth onset in mountain grasslands typically occurred from the second half of April in
218 the 1350 m - 1650 m elevation band (mean DOY of 112) to the first half of June in the 2250 m - 2550
219 m elevation band (mean DOY of 157) (Table 1). The date of maximum canopy greenness followed
220 around 1.5 months later, with the length of the growing period (TNDVImax-ONSET) decreasing
221 with elevation (Table 1). Late season phenology demonstrated a much larger range of inter-annual
222 variability – with a coefficient of variation ranging from 18% to 31% for senescence and regrowth –
223 as compared to those of Onset, TNDVImax and NDVImax (Table 1, Fig. 5), and this was observed
224 across all elevation bands (Table 1). Overall, year-to-year variations in phenology were much
225 smaller than those of HWI and P-ET₀ (Table 1).

226 The last four years (2013-2016) were among the five greenest summers of the study period,
227 while the four strongest negative anomalies of NDVImax occurred before 2006 (Fig. 5D). The
228 summers of 2003 and 2012 were characterized by an above normal senescence and a lack of
229 regrowth, although the NDVImax was close to normal (Fig. 5D, E, F). A lack of regrowth was also
230 observed in 2016, although senescence was close to normal and NDVImax was particularly high
231 (Fig. 5D, E, F). By comparison, the year 2015 exhibited a below normal senescence and above
232 normal regrowth and NDVImax (Fig. 5D, E, F).

233 Figure 6 shows the bivariate relationships among phenological anomalies and illustrates the
234 particularity of the four years marked by heat wave occurrence. We found a strong positive
235 relationship between anomalies of Onset and of TNDVImax (Table 2, Fig. 6A). The SMA slope was
236 significantly below one indicating that maximum canopy greenness was reached in a shorter time in
237 case of a delayed onset (Table 2). In addition, the two years with early season drought (e.g., 2003
238 and 2012) exhibited an earlier peak of NDVI than the one predicted by the SMA (Fig. 6A). The
239 relationship between TNDVImax and NDVImax showed that a delayed phenology tend to be
240 associated with higher values of NDVImax (Table 2, Fig. 6B). Remarkably, the two years with a
241 pronounced early season heat wave (e.g., 2003 and 2015) exhibited a higher anomaly of NDVImax
242 than predicted (Fig. 6B). Finally, we found a significant negative relationship between SEN (A60)
243 and REG (A60) (Table 2, Fig. 6C). The years 2003, 2012 and 2016 exhibited a late-season
244 phenology that was marked by normal to rapid senescence and limited regrowth while the year 2015
245 clearly showed an opposite pattern (Fig. 6C).

246 Finally, we examined the effects of HWI and P-ET₀ on phenology using multiple regression
247 models. For this quantitative analysis, we distinguished between the two periods, i.e. before and after
248 the peak, and among different elevation bands. Irrespective of elevation, there was a significant
249 effect of P-ET₀ (B30) anomalies on NDVImax while no effect was detected for HWI (B30) (Table 3,
250 Fig. 7A, B). Wetter conditions in the early season significantly enhanced the growth of grassland

251 while heat waves did not. P-ET₀ after the peak was also a significant driver of SEN (A60) and REG
252 (A60) and the magnitude of this effect markedly differed among elevation bands. Wet summers
253 significantly slowed down senescence and enhanced regrowth at low elevation, with up to 47% of
254 variance explained in SEN (A60) and 24% of variance explained in REG (A60) in the 1350 m 1650
255 m elevation band (Table 3, Fig. 7C, E). These effects vanished higher up and became non-significant
256 (SEN) or marginally significant (REG) above 2250 m (Table 3). Regarding HWI, we only found a
257 significant and negative effect on senescence above 2250 m (Table 3). Noticeably, the effect of late-
258 season heat waves on senescence depended on elevation with an increased senescence at low
259 elevation (although not significantly) and a delayed senescence at high elevation (Fig. 7D).

260 Overall, these results indicated that maximum canopy greenness, senescence and regrowth
261 were much more responsive to summer water balance than to heat waves. This is consistent with our
262 initial hypotheses concerning the combined effects of heat wave and climatic water deficit on plant
263 phenology. An early heat wave that did not coincide with a severe drought - as in 2015 and 2016 -
264 did not significantly impact NDVImax. A late heat wave coinciding with a severe drought - as in
265 2003, 2012 and 2016 - resulted in an increased senescence and a low regrowth. A late heat wave not
266 accompanied by a pronounced drought – as in 2015 - induced a delayed senescence, especially at
267 high elevation, and a substantial regrowth.

268 **Discussion**

269

270 Our study of mountain grassland phenology in the French Alps for the period from 2000 to 2016
271 has provided the framework to analyse more thoroughly how these ecosystems respond to heat
272 waves. Using data from the past two decades, we could show that (i) warmer summers generally
273 have a positive effect on mountain canopy greenness especially at high elevation, (ii) water deficit
274 hinders the positive temperature effect of heat waves on canopy greenness, and (iii) faster senescence
275 and weaker late-season regrowth are the main negative effects of heat waves that co-occur with
276 water deficit. Our findings emphasize the need to consider both the growth and senescent phases to

277 capture the effect of climate extremes on phenology. We also highlighted the pivotal role of the
278 magnitude of summer water balance and its within-summer distribution for understanding whether
279 mountain grasslands can benefit or not from higher summer temperatures.

280 We found a general increase in canopy greenness (NDVImax) in the French Alps during the study
281 period (2000-2016) which is consistent with our previous remote sensing study that showed a
282 greening trend for high-elevation ecosystems in the Ecrins Massif (Carlson et al., 2017). This
283 greening has also been documented in other temperate mountains (Xu et al., 2011) as well as in the
284 arctic and sub-arctic (Jia et al., 2003; Forbes et al., 2010). The combination of earlier snow melt-out
285 date and higher summer temperatures has been put forward as the main driver of changes in primary
286 productivity (Jonas et al., 2008; Zhang et al., 2013a; Choler, 2015; Dedieu et al., 2016; Choler,
287 2018). Besides temperature, other factors such as the increased deposition of atmospheric nitrogen
288 possibly led to some eutrophication of upland ecosystems and further contributed to greening
289 (Bowman et al., 2018). In alpine plants, nitrogen addition may induce stronger phenological changes
290 than warming alone (Smith et al., 2012). Our study indicated that sparsely vegetated meadows in the
291 French Alps are the most prone to greening, and we hypothesized that the prolonged growing season
292 in high-elevation contexts has created new thermally suitable niches for early plant colonizers which
293 could lead to an increase in primary productivity (Carlson et al., 2017). These conclusions are in
294 agreement with ground-based observations of community dynamics that emphasise the densification
295 of plant cover in open grasslands and/or the upward/northward shift of more productive functional
296 groups (Kullman, 2010; Myers-Smith et al., 2011; Steinbauer et al., 2018).

297 Our results also showed that the frequency of summer heat waves has increased over the last
298 decades in the French Alps. This is consistent with reports highlighting the increased probability of
299 heat waves in a warming climate (Stocker et al., 2013; Russo et al., 2014). We pointed out that the
300 four main heat waves that hit the Alps over the last 20 years did not have the same effect on
301 mountain grassland phenology. Remarkably, the 2015 heat wave had opposite late-season effects to

302 those of 2003, 2012, and 2016. This discrepancy is due to the combined effects of temperature and
303 climatic water balance, both in magnitude and timing. Water deficit coincided with heat wave in
304 2003 and 2012, and to a lesser extent in 2016. We hypothesize that a threshold in the water balance
305 was reached for these three years leading to the diminished canopy greenness during the late-season.
306 Other reports have suggested that the disproportionate effect of the 2003 summer heat wave may not
307 only be due to the unusually warm temperatures, but also to a negative soil water anomaly at the
308 beginning of the growth period (Loew et al., 2009). Compared to the lowland ecosystems, mountain
309 grasslands did not exhibit a strong reduction of NDVImax in 2003 and 2012, probably because the
310 snowmelt provided sufficient water for the initial growth period, at least in the Northern Alps.
311 Subsequently, the soil water content has likely decreased during the summer due to a climatic water
312 deficit causing a significant reduction of canopy greenness during the late-season. For the year 2015,
313 we hypothesize that the above normal water balance in the early season and the limited water deficit
314 in the late-season have favoured the positive effect of the late-season heat wave, especially for the
315 highest, i.e. the most temperature-limited, mountain grasslands. In their study of the 2003 heat wave,
316 Jolly et al. (2005) reported marked regional differences in the response of high elevation ecosystems.
317 In particular, it was striking that mountain ecosystems of the Southern Alps showed a reduced
318 canopy greenness compared to the Northern French or Swiss Alps, which was likely related to the
319 interplay of heat wave and water availability. Similarly, Cremonese et al. (2017) pointed out the co-
320 limitation of high temperature and soil water content to impede the greening of a *Nardus*-rich
321 grassland in 2015. Recent experimental studies conducted on temperate mountain grasslands showed
322 that the direct effects of air temperature on photosynthesis and aboveground phytomass production
323 strongly depend on soil water content (De Boeck et al., 2016). These findings should prompt us to
324 improve our understanding and regional modelling of the soil water balance of mountain grasslands.
325 Unfortunately, this remains notoriously difficult due to the many unknowns (e.g., the soil water
326 capacity and lateral run-offs). However, with further temperature increases looming in the not so

327 distant future, there is an urgent need to formulate eco-hydrological models of seasonal leaf
328 dynamics and to identify the different thresholds that drive ecosystem response. This is particularly
329 true for grasslands of the subalpine belt that are the most sensitive to drought and are a key resource
330 for summer livestock farming (Nettier et al., 2017)

331 Numerous studies on arctic and alpine ecosystems have underlined that the response to
332 warming varies across functional groups (Arft et al., 1999; Jonas et al., 2008; Jung et al., 2014;
333 Livensperger et al., 2016). In relation to the recent observed greening it is plausible that the
334 expansion of more productive habitats has changed the responsiveness of mountain grasslands to
335 climate extremes. The coexistence of a richer set of plant life forms may arise, e.g., through the
336 migration of low shrubs onto the grasslands, or of tall perennial grasses into otherwise low-stature
337 habitats. There are several lines of evidence that an increased functional diversity may provide some
338 ecosystem insurance by buffering the impact of environmental changes (Diaz and Cabido, 2001).
339 However, further studies are needed to examine a possible relationship between plant functional
340 diversity and the phenological responses of mountain grasslands to heat waves and drought. For
341 example, the combined use of high-resolution satellite imagery in combination with a regional-scale
342 database of vegetation could provide new insights into this line of enquiry.

343 Our comparative analysis of mountain grassland phenology over the last two decades
344 provides a knowledge base to help anticipate the long-term response of grasslands under future
345 climate conditions. Regional climate models used to compute climate projections are operating at
346 coarse resolutions (10-50 km) (Jacob et al., 2014) and are insufficient to provide ecologically-
347 relevant surface parameters in mountainous regions (Ford et al., 2013). Although downscaling
348 methods can refine projections of meteorological variables and snow cover dynamics (Verfaillie et
349 al., 2018), further work is needed to translate these model outputs into bioclimatic indicators and
350 assess to what extent they are driving canopy greenness. In the longer term, efforts have to be
351 conducted towards prognostic models of mountain grassland phenology that capture both

352 temperature and soil water constraints. The dynamics of leaf growth and senescence remains poorly
353 represented in land surface models (Arora and Boer, 2005; Richardson et al., 2013), and this holds
354 particularly true for seasonally snow-covered mountain grasslands. Our study has focused on inter-
355 annual fluctuations to provide a broad picture over the French Alps. Further work examining
356 between-site phenological variation along elevational and bioclimatic gradients will provide a
357 complementary view and will be helpful to improve our representation of the feedback between
358 phenology and climate within process-oriented models.
359

360 **Conclusions**

361 Our study highlighted the combined effect of summer temperature and water balance on the
362 phenology of temperate mountain grasslands. In the European Alps, the increased or prolonged
363 canopy greenness of mountain grasslands that result from warmer conditions becomes less
364 pronounced when water is limiting. While there has been a significant decadal-scale increase in both
365 the summer temperature and the frequency of heat waves, summer precipitation and reference
366 evapotranspiration did not show a similar trend and exhibited large inter-annual variability. In
367 addition, there is a growing body of evidence to support long-term changes of mountain vegetation in
368 relation to climate warming and land use change. The extent to which these changes modify the
369 sensitivity of mountain grassland to extreme events will also be pivotal to make possible the
370 prediction of canopy greenness under future climate.

371

372 **Acknowledgements**

373 Thanks are due to Brad Carlson for helpful discussions and to Deborah Verfaillie, Matthieu
374 Lafaysse and Matthieu Vernay (CNRM/CEN) for maintenance and provision of the SAFRAN
375 reanalysis used in this study. Comments and suggestions from the two reviewers have greatly
376 improved the manuscript. This research was conducted within the Long-Term Socio-Ecological
377 Research (LTSER) Zone Atelier Alpes, a member of the eLTER-Europe network. It received
378 funding from the LTSER Zone Atelier Alpes and from a scholarship of CONACYT. LECA and
379 CNRM/CEN are part of Labex OSUG@2020 (ANR10 LABX56).

380

381 **Tables**

382

383 **Table 1.** Annual means and inter-annual coefficients of variation (CV in %) of the meteorological
 384 and phenological variables used in the study.

Metric	Period	Abbreviation	Mean (CV)			
			1350 m - 1650 m	1650 m - 1950 m	1950 m - 2250 m	2250 m - 2550 m
<i>Meteorology</i>						
Heat Wave magnitude Index	Summer	HWI (JJA)	55 (79)	65 (71)	58 (79)	45 (89)
	Preceding the peak	HWI (B30)	18 (76)	21 (77)	20 (107)	14 (127)
	Following the peak	HWI (A60)	35 (111)	43 (98)	34 (116)	22 (130)
Precipitation – Reference Crop Evapotranspiration (mm)	Summer	P-ET ₀ (JJA)	61 (79)	58 (110)	51 (24)	16 (22)
	Preceding the peak	P-ET ₀ (B30)	35 (150)	24 (135)	14 (98)	5 (-285)
	Following the peak	P-ET ₀ (A60)	32 (25)	36 (-41)	39 (11)	25 (103)
<i>Phenology</i>						
Onset of growth (DOY)		ONSET	112 (8)	130 (8)	145 (8)	157 (7)
Date of maximum NDVI (DOY)		TNDVImax	175 (7)	184 (5)	192 (5)	200 (6)
Offset of growth (DOY)		OFFSET	327 (5)	315 (5)	306 (4)	300 (3)
Maximum NDVI		NDVImax	0.79 (2)	0.78 (2)	0.75 (3)	0.69 (4)
Senescence	Following the peak	SEN (A60)	0.13 (22)	0.14 (18)	0.16 (18)	0.19 (21)
Regrowth	Following the peak	REG (A60)	69 (18)	62 (19)	54 (24)	48 (31)

385

386 **Table 2.** Summary statistics for Standardized Major Axis (SMA) regression analysis of phenological
 387 variables. Shown are correlation coefficients (r), estimates of slopes (a) and intercepts (b) with 95%
 388 confidence intervals, Mean Square Error (MSE) and Mean Absolute Error (MAE). For the intercept,
 389 (NS) indicates a non-significant offset. For the slope, (NS) indicates an estimate statistically
 390 indistinguishable from one.

Relation	n	r	SMA intercept (b)	H ₀ : b=0 P value	SMA slope (a)	H ₀ : a=1 P value	MSE	MAE
ONSET - TNDVImax	1479	0.69	-0.11 (-0.13, -0.08)	***	0.73 (0.7, 0.76)	***	0.39	0.50
TNDVImax - NDVImax	1479	0.31	0.04 (0.01, 0.08)	*	0.97 (0.93, 1.02)	NS	0.51	0.55
SEN (A60) - REG (A60)	1478	-0.45	-0.1 (-0.16, -0.05)	***	-1.82 (-1.74, -1.91)	***	1.70	1.06

391

392 **Table 3.** Regression coefficients and adjusted R^2 for the linear models testing the effect of P-ET₀ and
 393 HWI on NDVImax, SEN (A60) and REG (A60). (x) denotes the interaction between the two effects.
 394 Plain text is for highly significant effect ($P < 0.001$), italics is for significant effect ($P < 0.01$). Empty
 395 cells indicate non-significant effects.

Effect	NDVImax			
	1350 m - 1650 m	1650 m - 1950 m	1950 m - 2250 m	2250 m - 2550 m
Intercept	-0.002	0.002	-0.043	-0.051
P-ET ₀ (B30)	0.27	0.33	0.25	0.14
HWI (B30)				
P-ET ₀ (B30) x HWI (B30)	0.16	0.15		
Adjusted R^2	0.14	0.16	0.11	0.04

Effect	SEN (A60)				REG (A60)			
	1350 m - 1650 m	1650 m - 1950 m	1950 m - 2250 m	2250 m - 2550 m	1350 m - 1650 m	1650 m - 1950 m	1950 m - 2250 m	2250 m - 2550 m
Intercept	-0.191	-0.147	-0.088	-0.042	0.108	0.016	-0.067	0.082
P-ET ₀ (A60)	-0.37	-0.27	-0.20		0.57	0.59	0.51	0.26
HWI (A60)				-0.18				
P-ET ₀ (A60) x HWI (A60)	-0.14	-0.08				-0.06	-0.21	
Adjusted R^2	0.47	0.33	0.08	0.05	0.24	0.24	0.20	0.05

396

397 **Supplementary Table 1.** Number of MODIS pixels by massif and elevation band.

Massif	Elevation band				Total
	1350 m - 1650 m	1650 m - 1950 m	1950 m - 2250 m	2250 m - 2550 m	
1. Chablais	553	787	119	0	1459
2. Aravis	878	679	94	0	1651
3. Mont-Blanc	174	728	714	49	1665
4. Bauges	268	233	8	0	509
5. Beaufortin	373	1425	1562	234	3594
6. Haute-Tarentaise	68	277	580	404	1329
7. Chartreuse	71	132	1	0	204
8. Belledonne	97	788	365	4	1254
9. Maurienne	296	1054	1179	430	2959
10. Vanoise	162	457	1572	899	3090
11. Haute-Maurienne	64	215	979	1181	2439
12. Grandes Rousses	415	1258	1529	622	3824
13. Tabor	75	274	717	636	1702
14. Vercors	561	324	4	0	889
15. Oisans	499	967	818	55	2339
16. Pelvoux	194	251	564	583	1592
17. Queyras	63	254	679	1489	2485
18. Devoluy	644	460	28	1	1133
19. Champsaur	601	651	918	419	2589
20. Embrunnais Parpaillon	113	165	523	454	1255
21. Ubaye	50	185	416	355	1006
22. Haut-Var Haut-Verdon	356	707	794	185	2042
23. Mercantour	342	946	1481	517	3286
Total	6917	13217	15644	8517	44295

398

399 **Figure legends**

400

401 **Figure 1.** (A) Study area showing the 23 SAFRAN massifs in the French Alps and the distribution of
402 the 250 m-resolution MODIS pixels ($n = 44,295$) dominated by mountain grasslands. (B) Pixel
403 distribution by massif and elevation band. Names of massifs are: 1. Chablais; 2. Aravis; 3. Mont-
404 Blanc; 4. Bauges; 5. Beaufortin; 6. Haute-Tarentaise; 7. Chartreuse; 8. Belledonne; 9. Maurienne; 10.
405 Vanoise; 11. Haute-Maurienne; 12. Grandes Rousses; 13. Thabor; 14. Vercors; 15. Oisans; 16.
406 Pelvoux; 17. Queyras; 18. Devoluy; 19. Champsaur; 20. Embrunnais Parpaillon; 21. Ubaye; 22.
407 Haut-Var Haut-Verdon; 23. Mercantour. Account of pixels by massif and elevation band is given in
408 Fig. S2.

409

410 **Figure 2.** An idealized yearly course of vegetation index showing the different variables and periods
411 that were used to capture the phenology of the mountain grasslands.

412

413 **Figure 3.** Annual standardized anomalies of (A) the Heat Wave magnitude Index (HWI (JJA)) and
414 (B) the difference between precipitation and reference crop evapotranspiration ($P-ET_0$ (JJA)) during
415 summer in mountain grasslands located between 1950 m and 2250 m. Meteorological variables were
416 estimated using the SAFRAN reanalysis (see Materials and Methods for details). The study period of
417 mountain grassland phenology started in year 2000 (dashed line). Boxplots represent the median
418 (central bar), and the first and third quartiles, with whiskers showing the 95% confidence intervals.
419 Grey boxplots represent the four main summer heat waves (2003, 2012, 2015, and 2016).

420

421 **Figure 4.** Bivariate plots of standardized anomalies of HWI and $P-ET_0$ during (A) the 30 days before
422 (B30), and (B) the 60 days after (A60) the date of maximum NDVI (TNDVImax). Large dots
423 represent the four main summer heat waves (2003, 2012, 2015, and 2016).

424

425 **Figure 5.** Annual standardized anomalies of mountain grassland phenology: (A) onset of growth, (B)
426 date of maximum NDVI (TNDVImax), (C) offset of growth, (D) maximum canopy greenness
427 (NDVImax), (E) senescence during the 60 days following NDVImax (SEN (A60)), and (F) regrowth
428 during the 60 days following NDVImax (REG (A60)). Boxplots represent the median (central bar),
429 and the first and third quartiles, with whiskers showing the 95% confidence intervals. Grey boxplots
430 represent the four main summer heat waves (2003, 2012, 2015, and 2016).

431

432 **Figure 6.** Bivariate relationships between annual standardized anomalies of TNDVImax, NDVImax,
433 SEN (A60) and REG (A60). Standard Major Axis (SMA) regression lines are shown. Large dots
434 represent the four main summer heat waves (2003, 2012, 2015, and 2016).

435

436 **Figure 7.** Effect of HWI and P-ET₀ on: NDVImax (A, B), SEN (A60) (C, D) and REG (A60) (E, F).
437 Dependent and independent variables used in the linear models are standardized anomalies.
438 Anomalies of HWI have been log-transformed. Regression lines are shown for each elevation band
439 (see Materials and Methods for details).

440

441 **Supplementary Figure 1.** Sensitivity of Heat Wave magnitude Index (HWI) to the length of the
442 window (parameter n) used to estimate the threshold temperature value (Eq. 1 in Materials and
443 Methods). Shown are the relative changes in HWI estimates when n varies from 15 days to 13 days
444 (A), or from 15 days to 11 days (B).

445

446 **Supplementary Figure 2.** Annual time series of summer HWI and P-ET₀ for mountain grasslands
447 located between 1950m and 2250m. Boxplots represent the median (central bar), and the first and

448 third quartiles, with whiskers showing the 95% confidence intervals. Grey boxplots represent the
449 four main summer heat waves (2003, 2012, 2015, and 2016).

450 **References**

- 451 Allen, R.G., Pereira, L.S., Raes, D. and Smith, M., 1998. Crop evapotranspiration-Guidelines for computing crop water
452 requirements-FAO Irrigation and drainage paper 56. FAO, Rome, 300: 6541.
- 453 Arft, A.M., Walker, M.D., Gurevitch, J., Alatalo, J.M., Bret Harte, M.S., Dale, M., Diemer, M., Gugerli, F., Henry, G.H.R.,
454 Jones, M.H., Hollister, R.D., Jonsdottir, I.S., Laine, K., Levesque, E., Marion, G.M., Molau, U., Molgaard, P.,
455 Nordenhall, U., Raszhivin, V., Robinson, C.H., Starr, G., Stenstrom, A., Stenstrom, M., Totland, O., Turner,
456 P.L., Walker, L.J., Webber, P.J., Welker, J.M. and Wookey, P.A., 1999. Responses of tundra plants to
457 experimental warming: Meta-analysis of the international tundra experiment. *Ecol. Monogr.*, 69(4): 491-511.
- 458 Arora, V.K. and Boer, G.J., 2005. A parameterization of leaf phenology for the terrestrial ecosystem component of
459 climate models. *Global Change Biol.*, 11(1): 39-59.
- 460 Beniston, M., Farinotti, D., Stoffel, M., Andreassen, L.M., Coppola, E., Eckert, N., Fantini, A., Giacona, F., Hauck, C.,
461 Huss, M., Huwald, H., Lehning, M., Lopez-Moreno, J.-I., Magnusson, J., Marty, C., Moran-Tejeda, E., Morin,
462 S., Naaim, M., Provenzale, A., Rabatel, A., Six, D., Stoetter, J., Strasser, U., Terzago, S. and Vincent, C., 2018.
463 The European mountain cryosphere: a review of its current state, trends, and future challenges.
464 *Cryosphere*, 12(2): 759-794.
- 465 Bowman, W.D., Ayyad, A., Bueno de Mesquita, C.P., Fierer, N., Potter, T.S. and Sternagel, S., 2018. Limited
466 ecosystem recovery from simulated chronic nitrogen deposition. *Ecological applications* : a publication of
467 the Ecological Society of America.
- 468 Cannone, N. and Pignatti, S., 2014. Ecological responses of plant species and communities to climate warming:
469 upward shift or range filling processes? *Clim. Change*, 123(2): 201-214.
- 470 Carlson, B.Z., Corona, M.C., Dentant, C., Bonet, R., Thuiller, W. and Choler, P., 2017. Observed long-term greening of
471 alpine vegetation-a case study in the French Alps. *Environmental Research Letters*, 12(11).
- 472 Choler, P., 2015. Growth response of temperate mountain grasslands to inter-annual variations in snow cover
473 duration. *Biogeosciences*, 12(12): 3885-3897.

474 Cholera, P., 2018. Winter soil temperature dependence of alpine plant distribution: Implications for anticipating
475 vegetation changes under a warming climate. *Perspectives in Plant Ecology Evolution and Systematics*, 30:
476 6-15.

477 Cholera, P., Sea, W., Briggs, P., Raupach, M. and Leuning, R., 2010. A simple ecohydrological model captures
478 essentials of seasonal leaf dynamics in semi-arid tropical grasslands. *Biogeosciences*, 7(3): 907-920.

479 Cremonese, E., Filippa, G., Galvagno, M., Siniscalco, C., Oddi, L., di Cella, U.M. and Migliavacca, M., 2017. Heat wave
480 hinders green wave: The impact of climate extreme on the phenology of a mountain grassland. *Agric. For.
481 Meteorol.*, 247: 320-330.

482 De Boeck, H.J., Bassin, S., Verlinden, M., Zeiter, M. and Hiltbrunner, E., 2016. Simulated heat waves affected alpine
483 grassland only in combination with drought. *New Phytol.*, 209(2): 531-541.

484 Dedieu, J.-P., Carlson, B.Z., Bigot, S., Sirguey, P., Vionnet, V. and Cholera, P., 2016. On the Importance of High-
485 Resolution Time Series of Optical Imagery for Quantifying the Effects of Snow Cover Duration on Alpine
486 Plant Habitat. *Remote Sensing*, 8(6): 481-481.

487 Diaz, S. and Cabido, M., 2001. Vive la difference: plant functional diversity matters to ecosystem processes. *Trends in
488 Ecology and Evolution*, 16(11): 646-655.

489 Dunn, A.H. and de Beurs, K.M., 2011. Land surface phenology of North American mountain environments using
490 moderate resolution imaging spectroradiometer data. *Remote Sens. Environ.*, 115(5): 1220-1233.

491 Durand, Y., Giraud, G., Laternser, M., Etchevers, P., Mérindol, L. and Lesaffre, B., 2009a. Reanalysis of 47 Years of
492 Climate in the French Alps (1958–2005): Climatology and Trends for Snow Cover. *Journal of Applied
493 Meteorology and Climatology*, 48(12): 2487-2512.

494 Durand, Y., Laternser, M., Giraud, G., Etchevers, P., Lesaffre, B. and Merindol, L., 2009b. Reanalysis of 44 Yr of
495 Climate in the French Alps (1958-2002): Methodology, Model Validation, Climatology, and Trends for Air
496 Temperature and Precipitation. *Journal of Applied Meteorology and Climatology*, 48(3): 429-449.

497 Fontana, F., Rixen, C., Jonas, T., Aberegg, G. and Wunderle, S., 2008. Alpine grassland phenology as seen in AVHRR,
498 VEGETATION, and MODIS NDVI time series - a comparison with in situ measurements. *Sensors*, 8(4): 2833-
499 2853.

500 Forbes, B.C., Macias Fauria, M. and Zetterberg, P., 2010. Russian Arctic warming and 'greening' are closely tracked
501 by tundra shrub willows. *Global Change Biol.*, 16(5): 1542-1554.

502 Ford, K.R., Ettinger, A.K., Lundquist, J.D., Raleigh, M.S. and Lambers, J.H.R., 2013. Spatial Heterogeneity in
503 Ecologically Important Climate Variables at Coarse and Fine Scales in a High-Snow Mountain Landscape.
504 Plos One, 8(6).

505 Gallinat, A.S., Primack, R.B. and Wagner, D.L., 2015. Autumn, the neglected season in climate change research.
506 Trends Ecol. Evol., 30(3): 169-176.

507 Garonna, I., de Jong, R., Stockli, R., Schmid, B., Schenkel, D., Schimel, D. and Schaepman, M.E., 2018. Shifting relative
508 importance of climatic constraints on land surface phenology. Environmental Research Letters, 13(2).

509 Gobiet, A., Kotlarski, S., Beniston, M., Heinrich, G., Rajczak, J. and Stoffel, M., 2014. 21st century climate change in
510 the European Alps-A review. Sci. Total Environ., 493: 1138-1151.

511 Gottfried, M., Pauli, H., Futschik, A., Akhalkatsi, M., Barancok, P., Alonso, J.L.B., Coldea, G., Dick, J., Erschbamer, B.,
512 Calzado, M.R.F., Kazakis, G., Krajci, J., Larsson, P., Mallaun, M., Michelsen, O., Moiseev, D., Moiseev, P.,
513 Molau, U., Merzouki, A., Nagy, L., Nakhutsrishvili, G., Pedersen, B., Pelino, G., Puscas, M., Rossi, G., Stanisci,
514 A., Theurillat, J.P., Tomaselli, M., Villar, L., Vittoz, P., Vogiatzakis, I. and Grabherr, G., 2012. Continent-wide
515 response of mountain vegetation to climate change. Nature Climate Change, 2(2): 111-115.

516 Hijmans, R.J., 2017. raster: Geographic Data Analysis and Modeling. R package version 2.6-7. [https://CRAN.R-](https://CRAN.R-project.org/package=raster)
517 [project.org/package=raster](https://CRAN.R-project.org/package=raster).

518 Inglada, J., Vincent, A., Arias, M., Tardy, B., Morin, D. and Rodes, I., 2017. Operational High Resolution Land Cover
519 Map Production at the Country Scale Using Satellite Image Time Series. Remote Sensing, 9(1).

520 Jacob, D., Petersen, J., Eggert, B., Alias, A., Christensen, O.B., Bouwer, L.M., Braun, A., Colette, A., Deque, M.,
521 Georgievski, G., Georgopoulou, E., Gobiet, A., Menut, L., Nikulin, G., Haensler, A., Hempelmann, N., Jones,
522 C., Keuler, K., Kovats, S., Kroener, N., Kotlarski, S., Kriegsmann, A., Martin, E., van Meijgaard, E., Moseley,
523 C., Pfeifer, S., Preuschmann, S., Radermacher, C., Radtke, K., Rechid, D., Rounsevell, M., Samuelsson, P.,
524 Somot, S., Soussana, J.-F., Teichmann, C., Valentini, R., Vautard, R., Weber, B. and Yiou, P., 2014. EURO-
525 CORDEX: new high-resolution climate change projections for European impact research. Regional
526 Environmental Change, 14(2): 563-578.

527 Jia, G.S.J., Epstein, H.E. and Walker, D.A., 2003. Greening of arctic Alaska, 1981-2001. Geophys. Res. Lett., 30(20).

528 Jolly, W.M., Dobbertin, M., Zimmermann, N.E. and Reichstein, M., 2005. Divergent vegetation growth responses to
529 the 2003 heat wave in the Swiss Alps. Geophys. Res. Lett., 32(18): NIL_1-NIL_4.

530 Jonas, T., Rixen, C., Sturm, M. and Stoeckli, V., 2008. How alpine plant growth is linked to snow cover and climate
531 variability. *Journal of Geophysical Research-Biogeosciences*, 113(G3).

532 Jung, V., Albert, C.H., Violle, C., Kunstler, G., Loucougaray, G. and Spiegelberger, T., 2014. Intraspecific trait variability
533 mediates the response of subalpine grassland communities to extreme drought events. *J. Ecol.*, 102(1): 45-
534 53.

535 Kullman, L., 2010. Alpine flora dynamics - a critical review of responses to climate change in the Swedish Scandes
536 since the early 1950s. *Nord. J. Bot.*, 28(4): 398-408.

537 Lenoir, J., Gegout, J.C., Marquet, P.A., de Ruffray, P. and Brisse, H., 2008. A significant upward shift in plant species
538 optimum elevation during the 20th century. *Science*, 320(5884): 1768-1771.

539 Liu, Q., Piao, S.L., Janssens, I.A., Fu, Y.S., Peng, S.S., Lian, X., Ciais, P., Myneni, R.B., Penuelas, J. and Wang, T., 2018.
540 Extension of the growing season increases vegetation exposure to frost. *Nature Communications*, 9.

541 Livensperger, C., Steltzer, H., Darrouzet-Nardi, A., Sullivan, P.F., Wallenstein, M. and Weintraub, M.N., 2016. Earlier
542 snowmelt and warming lead to earlier but not necessarily more plant growth. *Aob Plants*, 8.

543 Loew, A., Holmes, T. and de Jeu, R., 2009. The European heat wave 2003: Early indicators from multisensoral
544 microwave remote sensing? *Journal of Geophysical Research-Atmospheres*, 114.

545 Marchin, R.M., McHugh, I., Simpson, R.R., Ingram, L.J., Balas, D.S., Evans, B.J. and Adams, M.A., 2018. Productivity of
546 an Australian mountain grassland is limited by temperature and dryness despite long growing seasons.
547 *Agric. For. Meteorol.*, 256: 116-124.

548 Myers-Smith, I.H., Forbes, B.C., Wilmsking, M., Hallinger, M., Lantz, T., Blok, D., Tape, K.D., Macias-Fauria, M., Sass-
549 Klaassen, U., Levesque, E., Boudreau, S., Ropars, P., Hermanutz, L., Trant, A., Collier, L.S., Weijers, S.,
550 Rozema, J., Rayback, S.A., Schmidt, N.M., Schaepman-Strub, G., Wipf, S., Rixen, C., Menard, C.B., Venn, S.,
551 Goetz, S., Andreu-Hayles, L., Elmendorf, S., Ravolainen, V., Welker, J., Grogan, P., Epstein, H.E. and Hik, D.S.,
552 2011. Shrub expansion in tundra ecosystems: dynamics, impacts and research priorities. *Environmental*
553 *Research Letters*, 6(4).

554 Nettier, B., Dobremez, L., Lavorel, S. and Brunschwig, G., 2017. Resilience as a framework for analyzing the
555 adaptation of mountain summer pasture systems to climate change. *Ecol. Soc.*, 22(4).

556 Perpignan Lamigueiro, O. and Hijmans, R., 2018. rasterVis. R package version 0.45. URL:
557 <http://oscarperpignan.github.io/rastervis/>.

558 Pettorelli, N., Vik, J.O., Mysterud, A., Gaillard, J.M., Tucker, C.J. and Stenseth, N.C., 2005. Using the satellite-derived
559 NDVI to assess ecological responses to environmental change. *Trends Ecol. Evol.*, 20(9): 503-510.

560 R Core Team, 2017. R: A language and environment for statistical computing. <http://www.R-project.org/>. R
561 Foundation for Statistical Computing, Vienna, Austria.

562 Richardson, A.D., Keenan, T.F., Migliavacca, M., Ryu, Y., Sonnentag, O. and Toomey, M., 2013. Climate change,
563 phenology, and phenological control of vegetation feedbacks to the climate system. *Agric. For. Meteorol.*,
564 169: 156-173.

565 Russo, S., Dosio, A., Graversen, R.G., Sillmann, J., Carrao, H., Dunbar, M.B., Singleton, A., Montagna, P., Barbola, P.
566 and Vogt, J.V., 2014. Magnitude of extreme heat waves in present climate and their projection in a warming
567 world. *Journal of Geophysical Research-Atmospheres*, 119(22): 12500-12512.

568 Savitzky, A. and Golay, M.J.E., 1964. Smoothing and Differentiation of Data by Simplified Least Squares Procedures.
569 *Analytical Chemistry*, 36: 1627-1639.

570 signal developers, 2013. signal: Signal processing. URL: <http://r-forge.r-project.org/projects/signal/>.

571 Smith, J.G., Sconiers, W., Spasojevic, M.J., Ashton, I.W. and Suding, K.N., 2012. Phenological Changes in Alpine Plants
572 in Response to Increased Snowpack, Temperature, and Nitrogen. *Arctic Antarctic and Alpine Research*,
573 44(1): 135-142.

574 Steinbauer, M.J., Grytnes, J.-A., Jurasinski, G., Kulonen, A., Lenoir, J., Pauli, H., Rixen, C., Winkler, M., Bardy-
575 Durchhalter, M., Barni, E., Bjorkman, A.D., Breiner, F.T., Burg, S., Czortek, P., Dawes, M.A., Delimat, A.,
576 Dullinger, S., Erschbamer, B., Felde, V.A., Fernandez-Arberas, O., Fossheim, K.F., Gomez-Garcia, D., Georges,
577 D., Grindrud, E.T., Haider, S., Haugum, S.V., Henriksen, H., Herreros, M.J., Jaroszewicz, B., Jaroszynska, F.,
578 Kanka, R., Kapfer, J., Klanderud, K., Kuhn, I., Lamprecht, A., Matteodo, M., di Cella, U.M., Normand, S.,
579 Odland, A., Olsen, S.L., Palacio, S., Petey, M., Piscova, V., Sedlakova, B., Steinbauer, K., Stockli, V., Svenning,
580 J.-C., Teppa, G., Theurillat, J.-P., Vittoz, P., Woodin, S.J., Zimmermann, N.E. and Wipf, S., 2018. Accelerated
581 increase in plant species richness on mountain summits is linked to warming. *Nature*, 556(7700): 231-+.

582 Stocker, T.F., Qin, D., Plattner, G., Tignor, M., Allen, S., Boschung, J., Nauels, A., Xia, Y., Bex, V. and Midgley, P., 2013.
583 *Climate change 2013: the physical science basis*. Intergovernmental panel on climate change, working
584 group I contribution to the IPCC fifth assessment report (AR5). New York.

585 Vannier, O. and Braud, I., 2012. Calcul d'une évapotranspiration de référence spatialisée pour la modélisation
586 hydrologique à partir des données de la réanalyse SAFRAN de Météo-France.

587 <https://irsteadoc.irstea.fr/cemoa/PUB00029135>. Rapport scientifique, Note de travail du plateau SOMME (Synergie
588 Observation Modélisation en Modélisation de l'Environnement) d'Envirhônalp.

589 Verfaillie, D., Lafaysse, M., Deque, M., Eckert, N., Lejeune, Y. and Morin, S., 2018. Multi-component ensembles of
590 future meteorological and natural snow conditions for 1500m altitude in the Chartreuse mountain range,
591 Northern French Alps. *Cryosphere*, 12(4): 1249-1271.

592 Warton, D. and Ormerod, J., 2007. smatr: (Standardised) Major Axis Estimation and Testing Routines. R package
593 version 2.1. <http://web.maths.unsw.edu.au/~dwardon>.

594 Wheeler, J.A., Hoch, G., Cortes, A.J., Sedlacek, J., Wipf, S. and Rixen, C., 2014. Increased spring freezing vulnerability
595 for alpine shrubs under early snowmelt. *Oecologia*, 175(1): 219-229.

596 Wickham, H., 2016. *ggplot2: Elegant Graphics for Data Analysis*. Springer-Verlag New York, 2016.

597 Xu, W.X., Gu, S., Zhao, X.Q., Xiao, J.S., Tang, Y.H., Fang, J.Y., Zhang, J. and Jiang, S., 2011. High positive correlation
598 between soil temperature and NDVI from 1982 to 2006 in alpine meadow of the Three-River Source Region
599 on the Qinghai-Tibetan Plateau. *International Journal of Applied Earth Observation and Geoinformation*,
600 13(4): 528-535.

601 Zhang, G., Zhang, Y., Dong, J. and Xiao, X., 2013a. Green-up dates in the Tibetan Plateau have continuously advanced
602 from 1982 to 2011. *Proc. Natl. Acad. Sci. U.S.A.*, 110(11): 4309-4314.

603 Zhang, L., Guo, H., Ji, L., Lei, L., Wang, C., Yan, D., Li, B. and Li, J., 2013b. Vegetation greenness trend (2000 to 2009)
604 and the climate controls in the Qinghai-Tibetan Plateau. *Journal of Applied Remote Sensing*, 7.

605

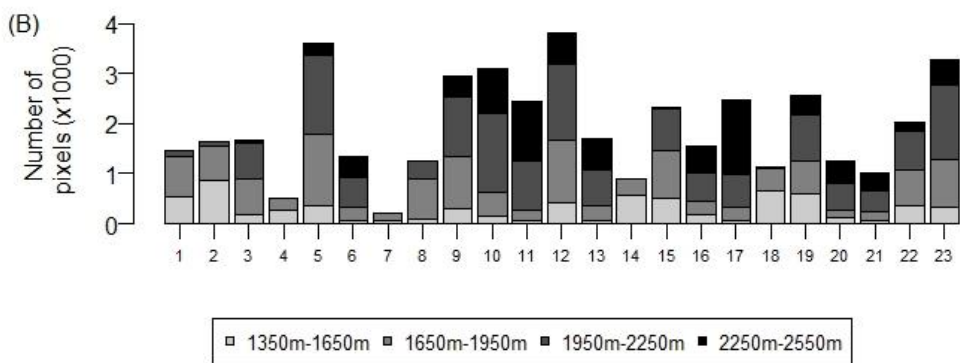
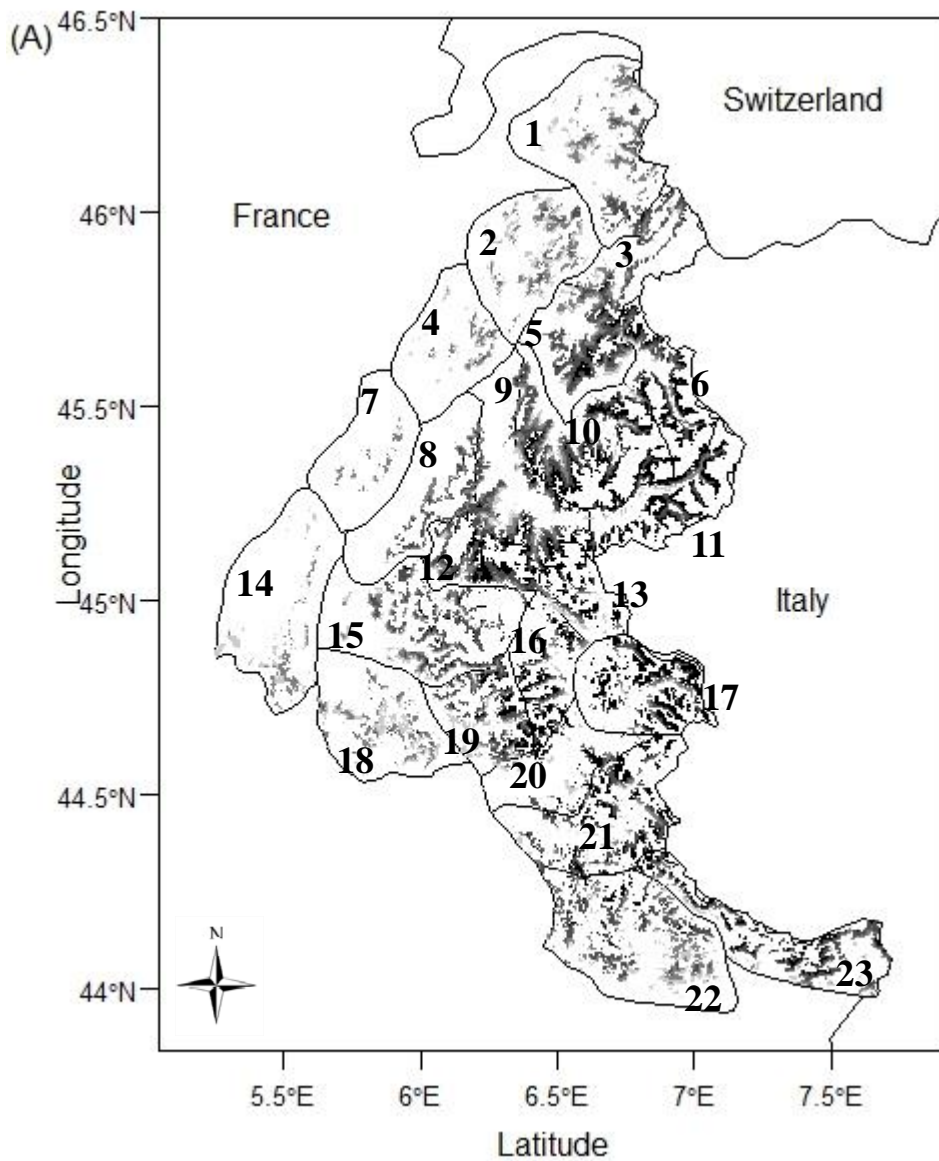


Figure 1

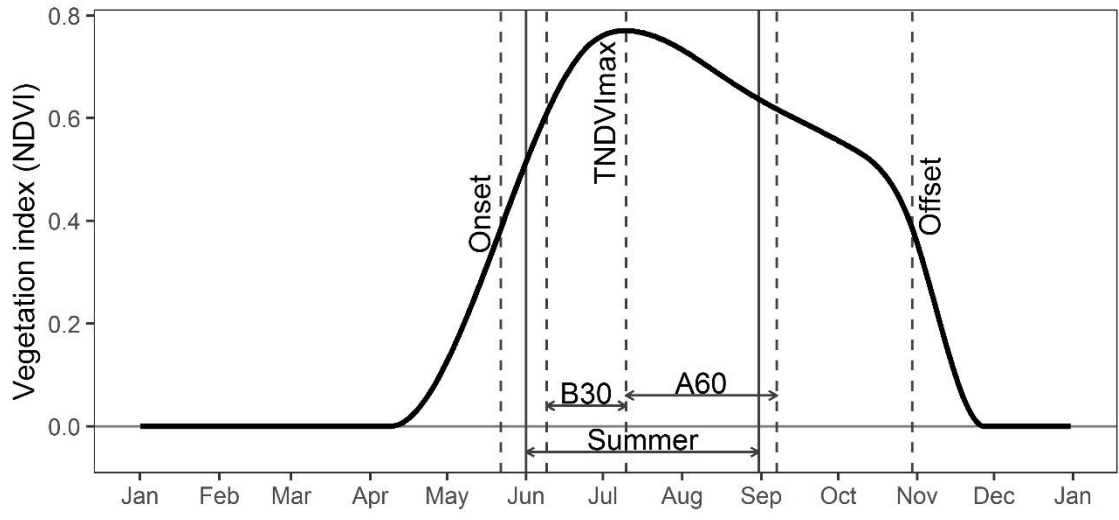


Figure 2

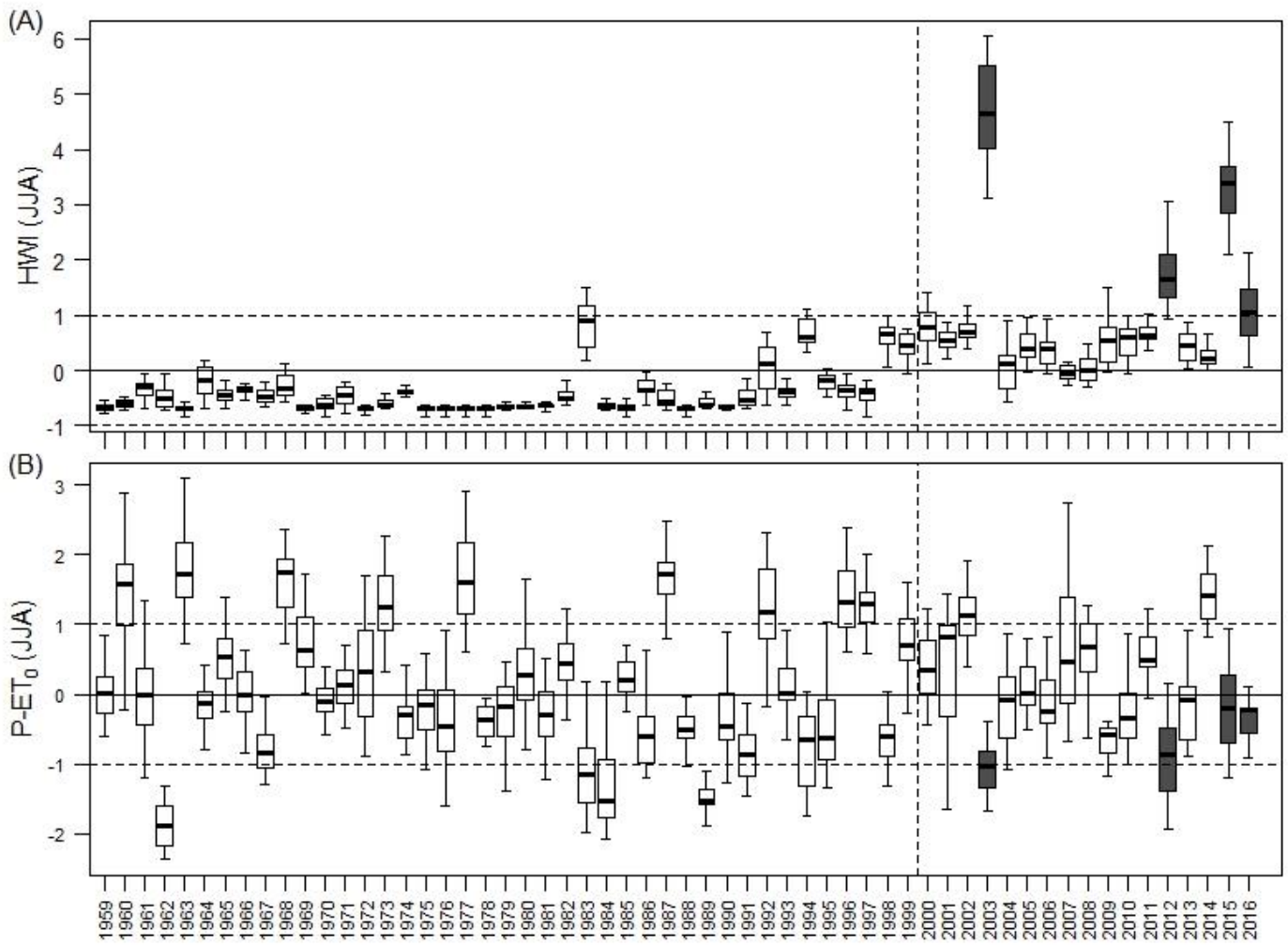


Figure 3

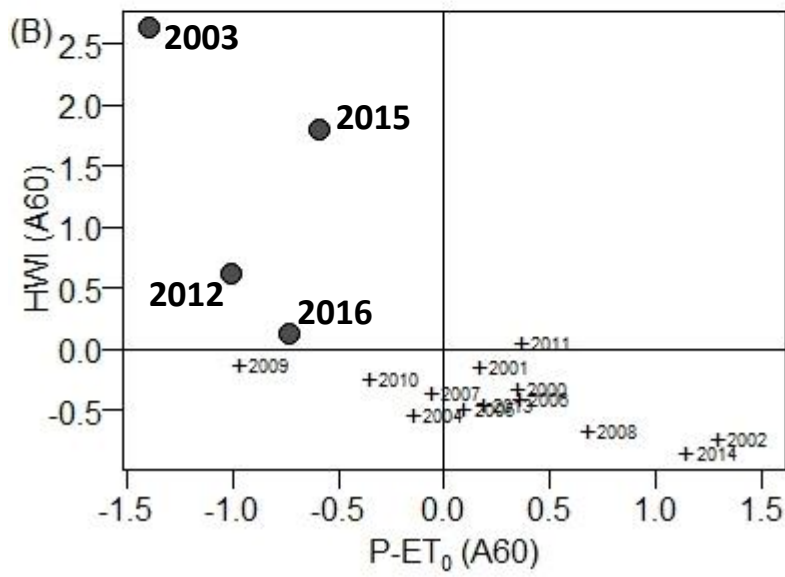
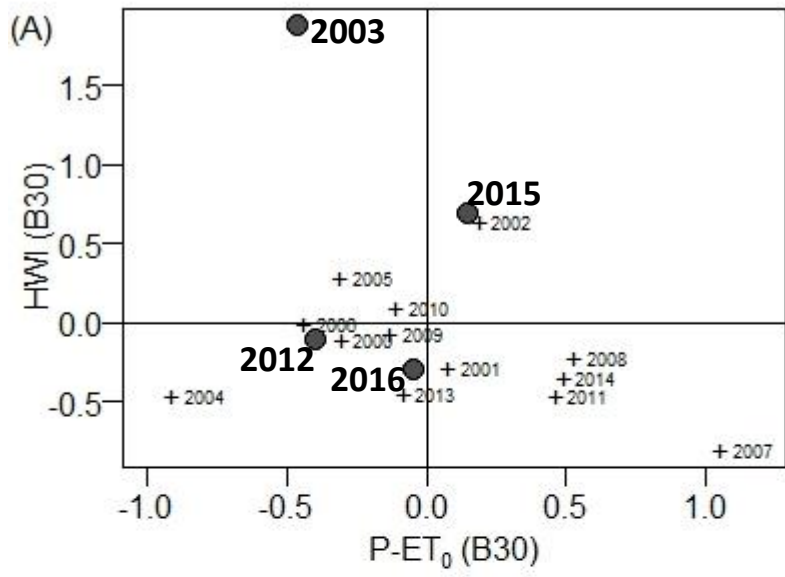


Figure 4

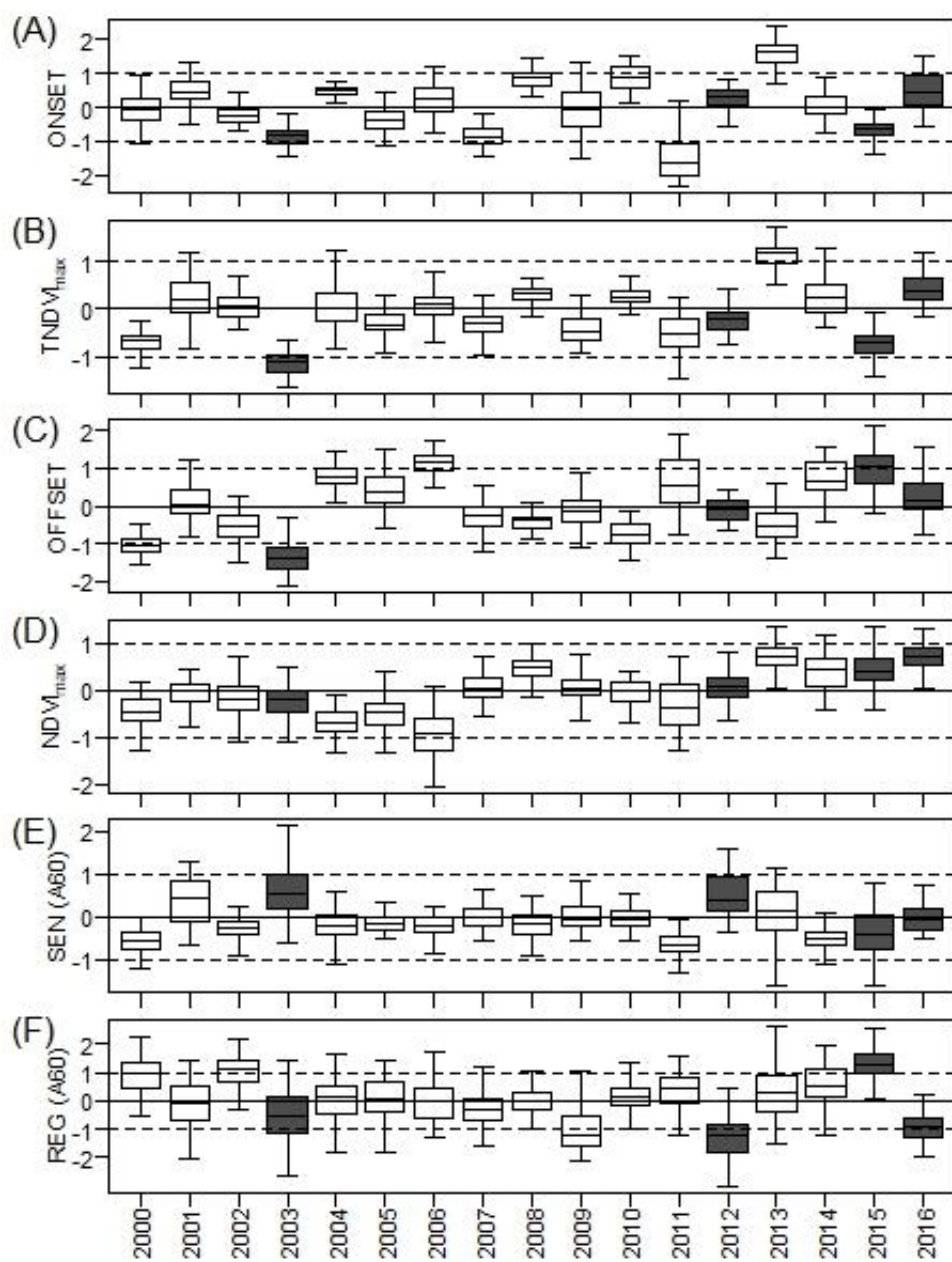


Figure 5

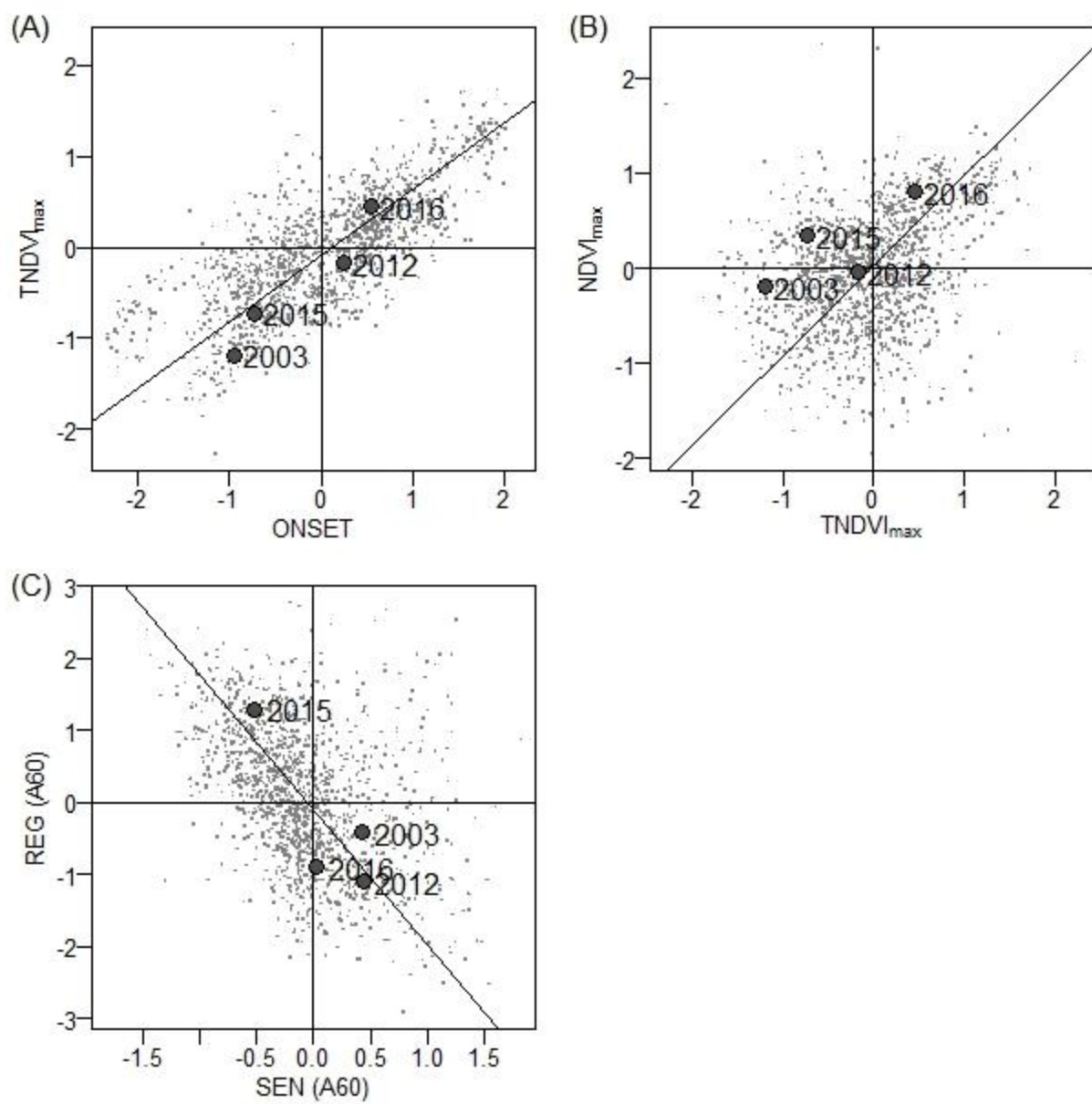


Figure 6

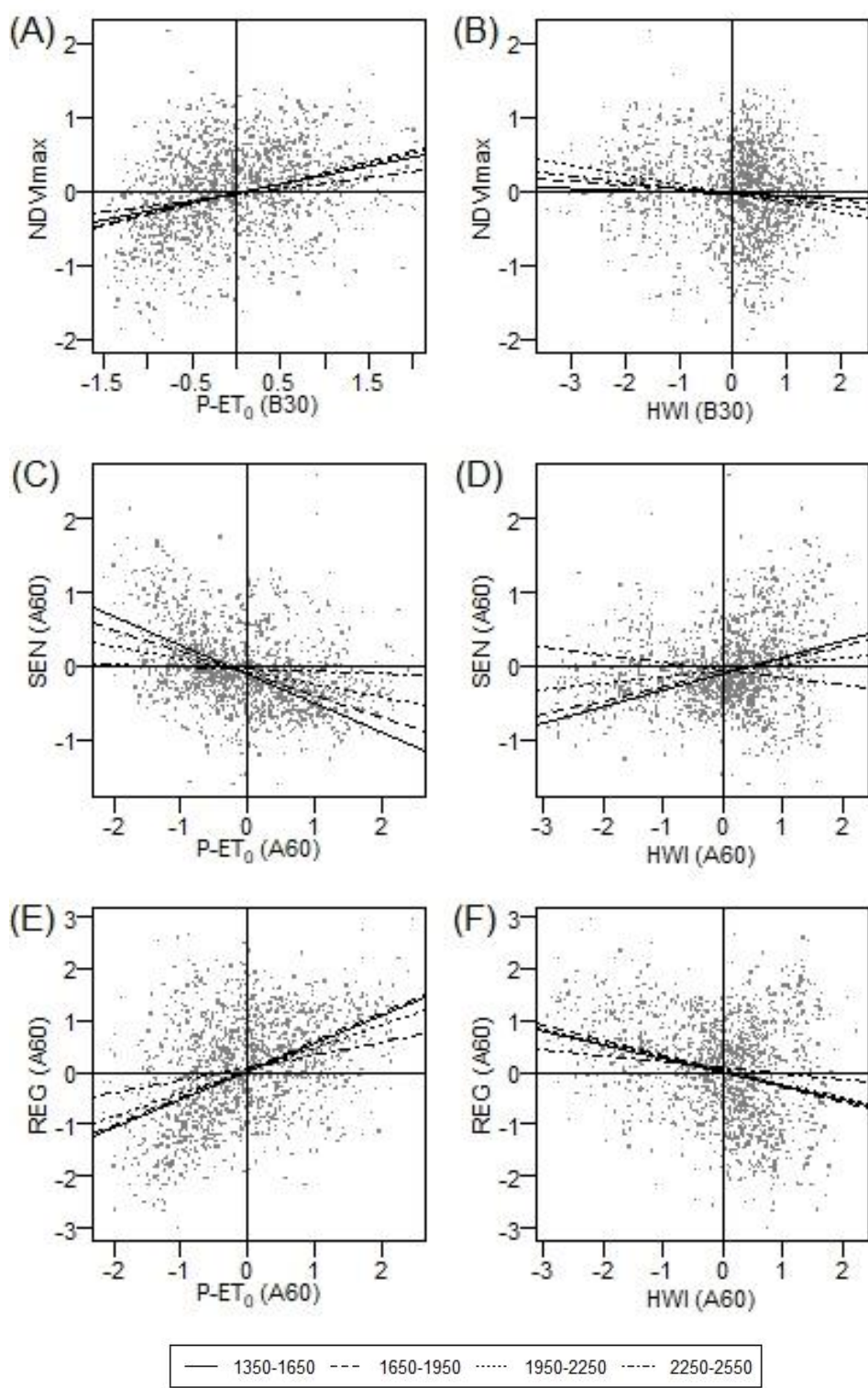


Figure 7

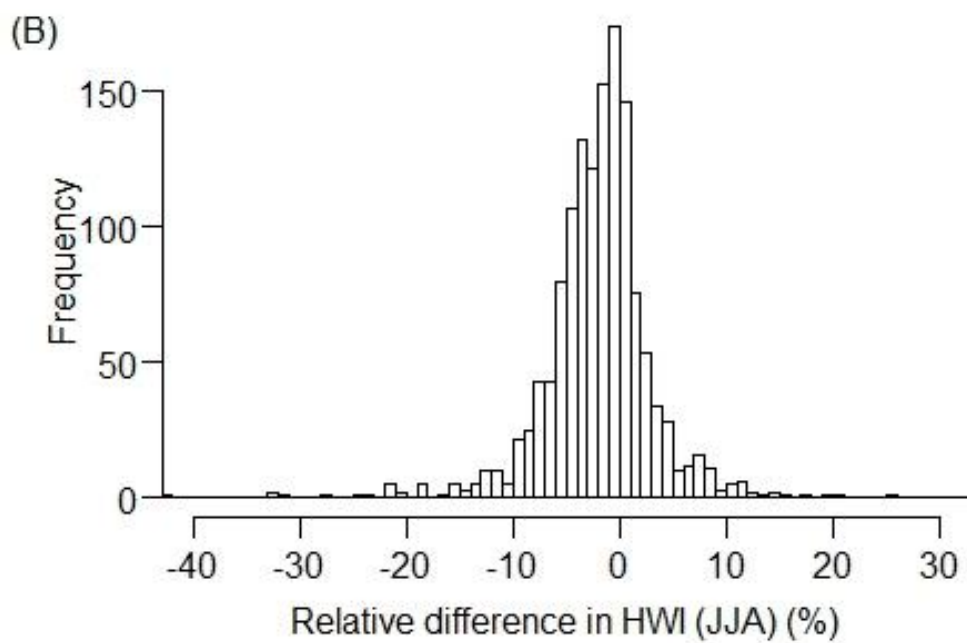
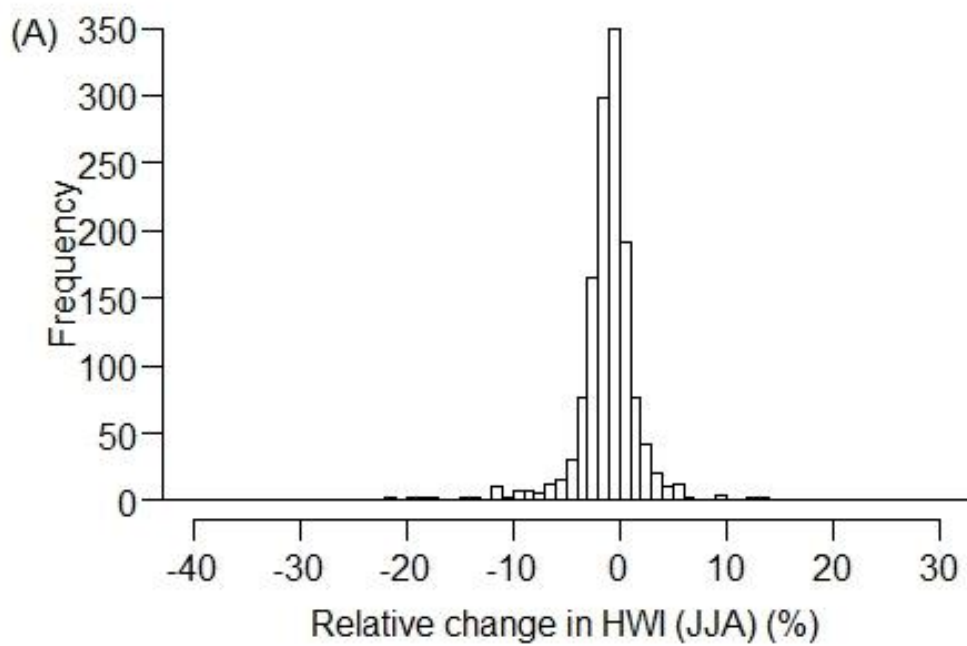


Figure S1

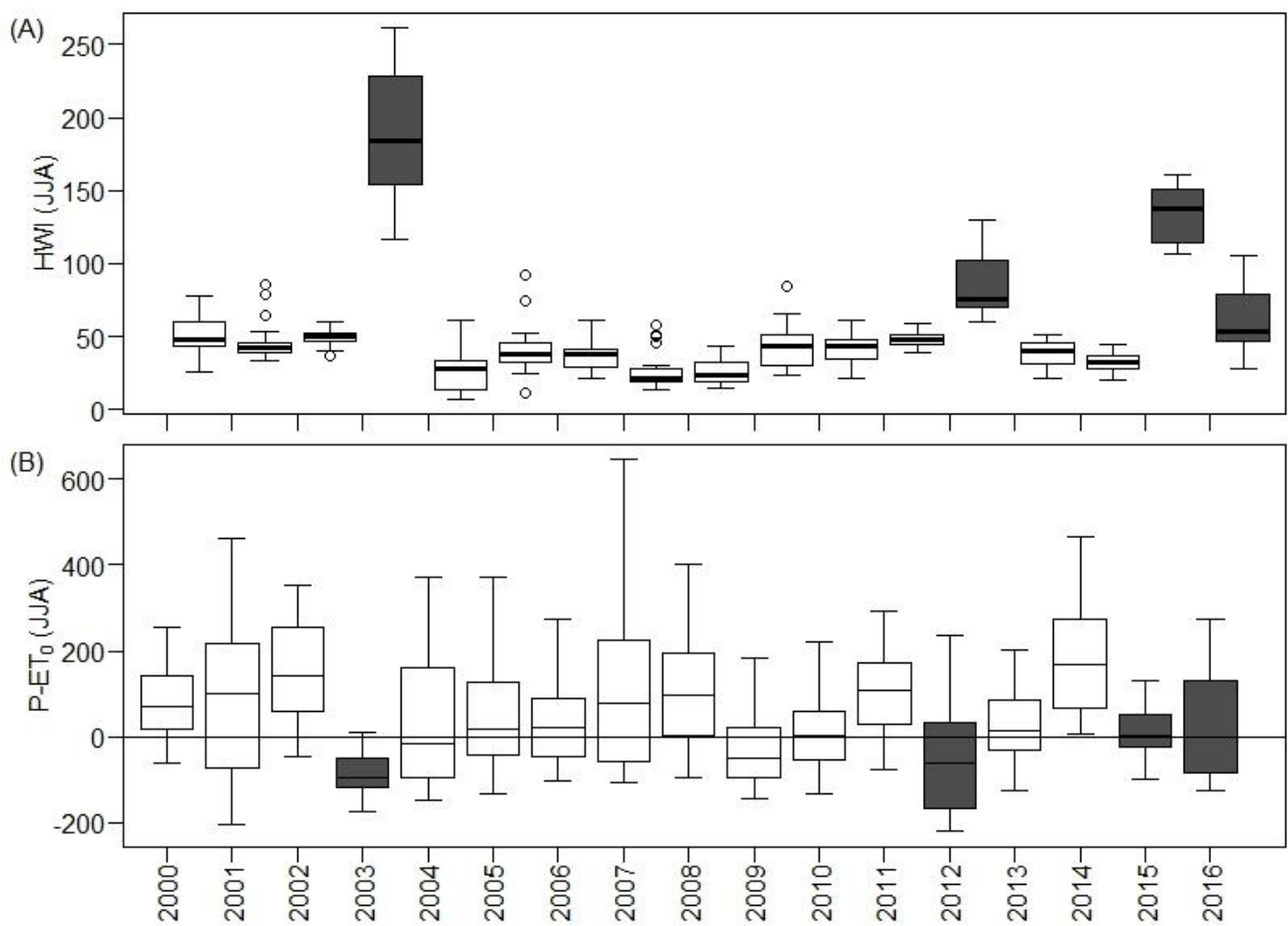


Figure S2